Epilepsy & Behavior 97 (2019) 229–243

Contents lists available at ScienceDirect

Epilepsy & Behavior

journal homepage: www.elsevier.com/locate/yebeh

Multiunit cluster firing patterns of piriform cortex and mediodorsal thalamus in absence epilepsy

James C. Young [a,b,*], Helen M. Nasser [a,b,d], Pablo M. Casillas-Espinosa [f,g,h], Terence J. O'Brien [f,g,h], Graeme D. Jackson [a,b,c], Antonio G. Paolini [a,b,d,e]

[a] The Florey Institute of Neuroscience and Mental Health, Melbourne, Australia
[b] Florey Department of Neuroscience and Mental Health, The University of Melbourne, Melbourne, Australia
[c] Department of Neurology, Austin Health, Melbourne, Australia
[d] ISN Psychology - Institute for Social Neuroscience, Melbourne, Australia
[e] School of Psychology and Public Health, La Trobe University, Melbourne, Australia
[f] Department of Neuroscience, Monash University, Melbourne, Australia
[g] Department of Medicine, The Royal Melbourne Hospital, The University of Melbourne, Australia
[h] Department of Neurology, The Royal Melbourne Hospital, The University of Melbourne, Australia

ARTICLE INFO

Article history:
Received 19 March 2019
Revised 9 May 2019
Accepted 20 May 2019
Available online 26 June 2019

Keywords:
Absence epilepsy
Multiunit clusters
Mediodorsal thalamus
Piriform cortex

ABSTRACT

Objective: The objective of the study were to investigate patterns of multiunit cluster firing in the piriform cortex (PC) and mediodorsal thalamus (MDT) in a rat model of genetic generalized epilepsy (GGE) with absence seizures and to assess whether these regions contribute to the initiation or spread of generalized epileptiform discharges.

Methods: Multiunit clusters and their corresponding local field potentials (LFPs) were recorded from microelectrode arrays implanted in the PC and MDT in urethane anesthetized Genetic Absence Epilepsy Rats from Strasbourg (GAERS) and nonepileptic control (NEC) rats. Peristimulus time histograms (PSTHs) and cross-correlograms were used to observe transient changes in both the rate of firing and synchrony over time. The phase locking of multiunit clusters to LFP signals (spike-LFP phase locking) was calculated for frequency bands associated with olfactory communication between the two brain regions.

Results: There were significant increases in both rate of firing and synchronous activity at the onset of generalized epileptiform discharges in both PC and MDT. Prior to and following these increases in synchronous activity, there were periods of suppression. Significant increases in spike-LFP phase locking were observed within the PC prior to the onset of epileptiform discharges across all spectral bands. There were also significant increases in spike-LFP phase locking within the theta band of the MDT prior to onset. Between the two brain regions, there was a significant decrease in spike-LFP phase locking −0.5 s prior to onset in the theta band which coincided with a significant elevation in spike-LFP phase locking in the gamma band.

Conclusions: Both the PC and MDT are engaged in the absence epilepsy network. Early spike-LFP phase locking between these two brain regions suggests potential involvement in the initiation of seizure activity.

1. Introduction

In the study of the pathophysiology of absence seizures in patients with genetic generalized epilepsy (GGE), there has been an intense focus on the role of corticothalamic networks in the epileptogenic process with little focus on the role of other brain regions. There is emerging evidence of mesial temporal structures playing a role in absence epilepsy including the piriform cortex (PC), a brain region responsible for olfactory processing [1–3]. Typically, mesial temporal lobe damage is associated with mesial temporal lobe epilepsy that manifests through epileptic dysfunction of the hippocampus, amygdala, entorhinal cortex, and the PC [3–6]. Mesial temporal lobe volume reduction has also been observed in patients with juvenile absence epilepsy [1] while preclinical studies have shown dysfunction in the hippocampus [7] and amygdala [8]. The Genetic Absence Epilepsy Rats from Strasbourg (GAERS) rat model during kindling has demonstrated increased blood flow in the somatosensory cortex and ventrobasal thalamus as well as the PC, amygdala, entorhinal cortex, and hippocampus (CA2)

Abbreviations: BOLD, blood oxygen-level dependent; EEG, electroencephalography; fMRI, functional magnetic resonance imaging; GAERS, Genetic Absence Epilepsy Rats from Strasbourg; GGE, genetic generalized epilepsy; LFP, local field potential; MDT, mediodorsal thalamus; MUA, multiunit activity; NEC, nonepileptic control; PC, piriform cortex; PSTH, peristimulus time histogram.

* Corresponding author at: The Florey Institute of Neuroscience and Mental Health, Melbourne Brain Centre, 245 Burgundy Street, Heidelberg, Victoria 3084, Australia.
E-mail address: james.young@unimelb.edu.au (J.C. Young).

https://doi.org/10.1016/j.yebeh.2019.05.032
1525-5050/

[9], suggesting relationship between thalamocortical and limbic structures in absence epilepsy [10]. There is also clinical evidence of bilateral activation of the PC occurring synchronously with generalized spike–wave discharges that are the electroencephalography (EEG) hallmark of absence seizures [3]. However, the PC's neuronal firing properties and engagement with other limbic structures involved in absence epilepsy are unknown.

The PC is known to be prone to hyperexcitable activity and displays notable connections to limbic structures as well as regions associated with absence epilepsy [11]. It displays strong excitatory projections towards the mediodorsal thalamus (MDT) [12–16], and olfactory communication between the two brain regions is thought to be achieved through neural oscillations in the theta (4–8 Hz), beta (13–30 Hz), and gamma (30–80 Hz) bands from field potential recordings [17–19]. Epileptic events in absence epilepsy are considered to be cortically driven [20,21], however, there is evidence to suggest that there is early involvement of subcortical structures such as the MDT [22,23]. The MDT is a higher-order thalamic relay, in contrast to the somatosensory cortex (first-order thalamic relay), that relays information between cortical regions which is essential for conscious operations and may be disrupted in absence epilepsy [24]. Higher-order thalamic relays typically fire after first-order thalamic relays [25] with the exception of the MDT, which has shown to fire prior to the peak of spike–wave discharges along with first-order thalamic nuclei and the reticular thalamic nuclei in an absence epilepsy rat model [22]. Furthermore, early activation of this region has also been demonstrated in humans with absence epilepsy in an EEG/functional magnetic resonance imaging (fMRI) study [26] and was found to be a key subregion of the thalamus that drove cortical activity to produce spike–wave discharges. The MDT has also demonstrated a significant increase in glutamatergic positive neurons in the GAERS [27], a well-established animal model of absence epilepsy [28,29], while lesions have also been reported in the MDT in patients with spike–wave discharges [30]. Finally, the MDT's connections with the reticular thalamic nuclei [31] may allow it to contribute to the absence epilepsy network [10].

The PC and MDT also display reciprocal connections with the orbitofrontal cortex forming a local circuit of physiological and potentially epileptic importance [32–34]. The orbitofrontal cortex has shown to locally generated absence seizures [35–37] and also receives sensory inputs from the somatosensory cortex [38], another critical region that cortically drives absence seizures [24,39–41]. Therefore, the PC and MDT may contribute to the generation of absence seizure activity via their connections to the orbitofrontal cortex and downstream projections to other prefrontal regions.

In order to confirm the involvement of the PC in absence epilepsy, it is necessary to study its multiunit firing patterns along with those of MDT because of its association with absence epilepsy and its strong inputs from the PC. Utilizing multichannel microelectrode arrays to record multiunit activity (MUA), we investigated the transient changes in excitability of the two regions and patterns of synchronous neuronal firing around the onset of epileptic events. Furthermore, by recording local field potentials (LFPs), we can also determine the degree of phase locking between multiunit clusters and the frequency bands (spike-LFP phase locking) associated with olfactory communication between the PC and the MDT. Changes in spike-LFP phase locking prior to the onset of absence seizures may be indicative of involvement of the PC–MDT pathway in absence epilepsy.

2. Material and methods

2.1. Experimental design and data collection

Experiments were conducted on adult rats (aged 4–6 months) from the GAERS strain and a nonepileptic controls (NECs) strain. All procedures were approved by Animal Ethics Committee at the Florey Institute of Neuroscience and Mental Health (FINMH-17005) in adherence to the Australian Code of Practice for the Care and Use of Animals for Scientific Purposes. Rats were housed on a 12-hour light/dark cycle with lights on at 9 am and were acclimatized for 1 week prior to any experiments commencing. All rats had free access to food and water. These rats were anesthetized with systemic Intraperitoneal (I.P.) injections of urethane (20% vol/vol) until the rats were unconscious. Rats were then placed in a stereotaxic frame with a thermoregulatory head pad to maintain body temperature at 37 °C. Burr holes were drilled over primary motor cortex (left and right) (coordinates Anterior-Posterior (AP): 10.44 mm, Medial-Lateral (ML): ±3.5 mm, Dorsal-Ventral (DV): 0 mm (from dura), angle: 0°) for insertion of stainless-steel screw electrodes (Plastics One) for EEG recordings. These coordinates are based on approximations from Paxinos and Watson [42]. The screw electrodes were mostly placed over primary motor cortex with some overlap at the neighboring somatosensory cortex. A 32-channel microelectrode arrays (Neuronexus) were inserted into the left PC (AP: 8.2 mm, ML: −4.9 mm, DV: 7.6 mm, angle: 0°) and left mediodorsal nucleus of the thalamus (AP: 9.0 mm, ML: −0.6 mm, DV: 6.5 mm, angle: 32.5°). Following completion of surgical procedures, rats underwent electrophysiological recordings for approximately 7 h. At the end of electrophysiological recordings, all animals were terminated with an 80-mg/kg dose of sodium pentobarbitone followed by transcardial perfusion. Rat brains were then preserved in 10% formalin. Tissue was sectioned at 10–20 μm and Nissl stained to verify placement of electrodes (Fig. 1). The placement of microelectrode arrays in the PC and MDT was verified using landmarks described in Paxinos and Watson [42] under a confocal microscope (Nikon, Australia) in 3 subjects while screw electrodes in motor cortex were confirmed via visual inspection. The bottom 16 electrode contacts of both the PC and MDT were used for analysis as they were consistently located in the correct position.

A Tucker-Davis Technologies system was utilized in the recording of multiunit cluster spikes, EEG, and LFPs. Recordings were amplified by a PZ2 PreAmp and were preprocessed on a RZ2 BioAmp Processor. Electroencephalography and LFP recordings were sampled at 4069 Hz. Multiunit activity was recorded between 300 and 5000 Hz of a field potential signal sampled at 24,414.14 Hz. Spike detection was performed by an online spike discriminator which would record 31 samples (1.2 ms) of the signal waveform that represents a single multiunit cluster spike. However, this results in the recording system not accurately tracking all spikes, since another spike could not be triggered for 31 samples. This online detection method, therefore, does not include spikes within close proximity (<31 samples) of one another. A rethresholding approach was applied offline to accurately detect potential missing spikes [43]. This was achieved by taking the 31 samples of multiunit cluster spikes and counting the number of samples that exceeded 1.5 standard deviations above the mean of the multiunit cluster. Data were stored onto an RS4 Data Streamer for analysis. MATLAB 2018 was used for postexperimental analysis of multiunit clusters, EEG and LFPs data.

For the awake freely moving GAERS recordings shown in Fig. 2, a different experiment protocol was performed. This procedure was approved by The Florey Animal Ethics committee (Ethics Number 14-053-UM). The animal was individually housed alternating 12-hour cycles of light and dark. Food and water were provided ad libitum for the whole duration of the study. At 20 weeks of age, the GAERS was anesthetized using isofluorane at 5% (Ceva isofluorane, Piramal Enterprises Limited, India) to start the surgery. The surgical procedure was done using an aseptic technique. Once the animal was anesthetized, Polyvisc (Frenchs Forest NSW, Australia) was applied to the eyes to prevent eye damage. The fur was shaved from the rat skull and thoracic-abdominal regions followed by cleaning of the skin using iodine (Riodine, Orion Laboratories, Balcatta, Australia), sterile water, and chlorhexidine (Johnson and Johnson, North Ryde, Australia). Then, a single midline incision was made on the scalp posterior to the eyes between the ears. Six burr holes were drilled through the skull without penetrating the dura, one on each side anterior to the bregma, two to each side anterior to lambda, and two to each side in the parietal

bones. Subdural recording electrodes were placed screwed into each hole. Each recording electrode comprised a 1.3-mm gold connector soldered onto a nickel alloy jeweler screw (Farnell Components, Chester Hill, Australia). The recording electrodes were fixed in position by applying Vertex dental cement around the electrodes and over the skull. The incision was then sutured using nylon (4/0, Surgical Specialties Australia). Immediately after surgery, each rat received an intraperitoneal injection of 1 ml/kg analgesic solution containing intraperitoneal carprofen. One week after surgery, the rat underwent two sessions of 24 h of continuous video-EEG recording per week. The rat was connected to the EEG recording with cables that allowed it free movement within the cage. The rat was habituated to the EEG recording setup for at least 1 h before the recordings. Electroencephalography recordings were obtained using Profusion 3 software (Compumedics, Australia), unfiltered and digitized at 512 Hz.

2.2. Generalized epileptiform discharge detection

Epileptic high amplitude 5–9 Hz generalized epileptiform discharges were observed on the EEG data recorded from screw electrodes. Fig. 2 demonstrates the typical spike–wave discharges in EEG recordings from an awake freely moving GAERS. The left screw electrode in the primary motor cortex was used for generalized discharge detection while the right screw electrode was used to confirm the discharges spread across both hemispheres of the brain. This is due to the PC and MDT microelectrode arrays being placed in the left hemisphere.

The EEG signal recorded from screw electrodes was bandpass filtered using a third-order Butterworth bandpass zero-phase filter within the 5 to 9 Hz frequency range. Following bandpass filtering, a moving average root mean square filter with a window size of 3 samples was applied to the filtered signal to detect the occurrence of generalized epileptiform discharges. This method has been previously utilized in electrophysiology event detection [44]. The onset time of generalized epileptiform discharges can be deduced by observing the intersection of the moving average root mean square signal with a threshold derived from the empirical cumulative distribution function of 5 s of baseline signal. This baseline signal was defined as a 5-second period at the center of an interictal period of at least 1 min in duration where no epileptic activity was observed. The 95th percentile of the empirical cumulative distribution function was used as the threshold value as this has been previously used in detection of high-frequency oscillations (HFOs) [45]. Following detection of generalized epileptiform discharges, we randomly selected 100 generalized epileptiform discharges from each GAERS, and 100 random second samples were selected from each NEC rat.

3. Multiunit cluster analysis

3.1. Spike rate

The rate of multiunit cluster firing is the temporal average of spiking obtained by counting the number of spikes for a given time bin. Changes in the spike rate can be visually represented by peristimulus time histograms (PSTHs) as shown in Fig. 3B. The spike rate can be determined over a single trial however at the expense of losing temporal resolution with regard to variations in neural response for a time course. Therefore, 100 trials were taken across 100 generalized epileptiform discharges and 100 randomly sampled 5-second periods of controls to construct PSTHs with bin sizes of 0.1 ms for individual multiunit clusters. Furthermore, the overall PSTH of a brain region can be constructed by counting the total number of spikes per bin for all multiunit clusters and trials and dividing by the total duration of recording.

3.2. Neural synchrony

Neural synchrony is an important measure of long range and local connectivity within brain regions and can be determined through the application of cross-correlograms to multiunit cluster pairs. Sensory and cognitive processes typically rely on the intensive activity of a large population of neurons, hence, why quantifying the neural synchrony of multiunit clusters can aid our understanding or predict the mechanisms of such processes [46]. The onset of epileptic events is well-known to be associated with hypersynchronous activity [47]. The application of neural synchrony is, therefore, important in determining not only the occurrence of epileptic events but also whether specific brain regions contribute to their initiation through patterns of either synchronous or asynchronous activity during a preonset state. Construction of neural synchrony profiles can be achieved by segmenting the analysis of neural synchrony into sliding windows, allowing us to observe temporal changes in both local and long-range connectivity. This process is detailed in Fig. 4 and the following sections.

3.2.1. Cross-correlogram construction and analysis

The cross-correlogram $R_{AB}(\tau)$ is defined as binning the distances in time between two multiunit clusters where τ represents the lag time. It is assumed that the spike trains analyzed are independent with a Poisson distribution of bin counts as has been previously conducted [48]. The expected values (E) and standard deviations (σ) of each cross-correlogram were computed (Eqs. (1) and (2)).

$$E = N_A N_B \Delta / T \tag{1}$$

$$\sigma = \sqrt{E} \tag{2}$$

where N_A and N_B are the number of spikes in the multiunit clusters A and B, Δ is the bin width (1 ms), and T (100 events $*$ 50 ms) is the duration of the recording for a single window. The peaks of the raw cross-correlograms were deemed significant if their Z-scores crossed a level of 4 times the standard deviation above the expected value [48]. The Z score is calculated as shown in Eq. (3).

$$Z_{AB}(\tau) = [R_{AB}(\tau) - E]/\sigma \tag{3}$$

To avoid errors where peaks cross 4 times the standard deviation threshold, only peaks where three consecutive bins cross the threshold at the center of the cross-correlogram are taken into account. These cross-correlograms are classified as significantly synchronous. The percentage of significant multiunit cluster pairs can then be determined by simply dividing the number of significant by the total number of multiunit cluster pairs. If a sliding window approach is applied to the multiunit cluster pairs, changes in the percentage of significantly synchronous pairs can be shown to change over time.

3.2.2. Quantifying neural synchrony

From the Z-score of the cross-correlograms, the correlation coefficient can be calculated as shown in Eq. (4) for any lag time that crosses the significantly synchronous threshold [48].

$$\rho(\tau) = Z_{AB}(\tau)\Delta / T \tag{4}$$

ρ is the correlation coefficient, $Z_{AB}(\tau)$ is the Z-score for multiunit clusters A and B for lag time τ, Δ is the bin width, and T is the duration. This correlation has previously been termed neural synchrony [43], however, it does not provide a single value for neural synchrony of a given cross-correlogram. The area A of the Z-score of the cross-correlogram which exceeds 4 (Eq. (5)) was instead utilized as an overall measure of neural synchrony. This is analogous to the area above the red

Electrode Implantation Sites

A) Mediodorsal Thalamus Electrode Placement – Coronal View

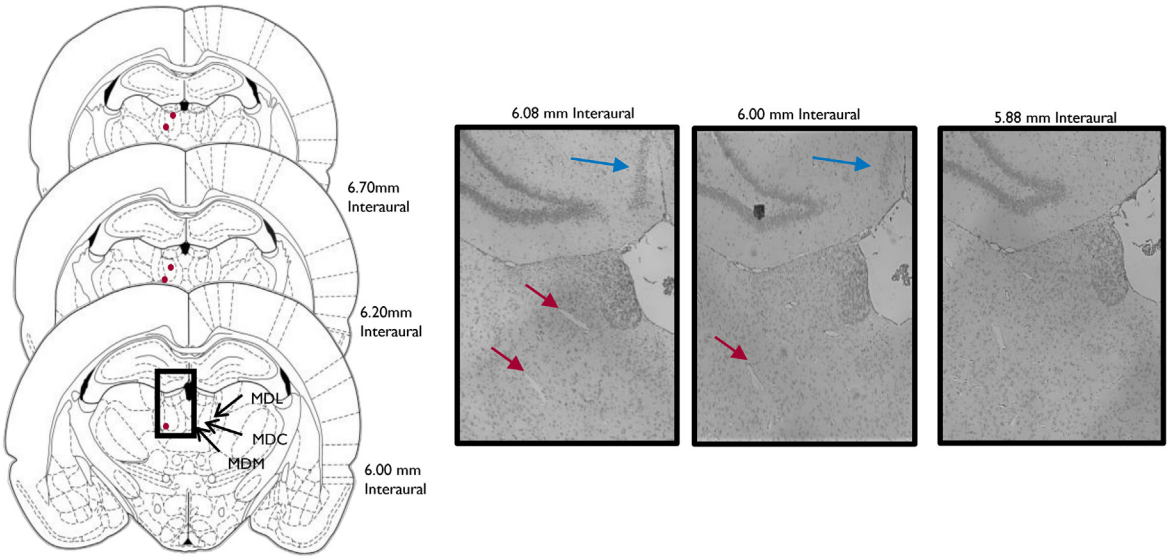

B) Piriform Cortex Electrode Placement – Coronal View

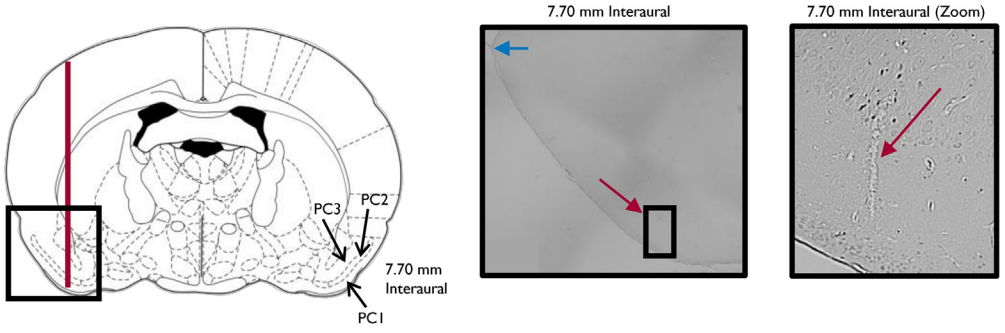

C) Electrode Placement – Sagittal View Reconstruction

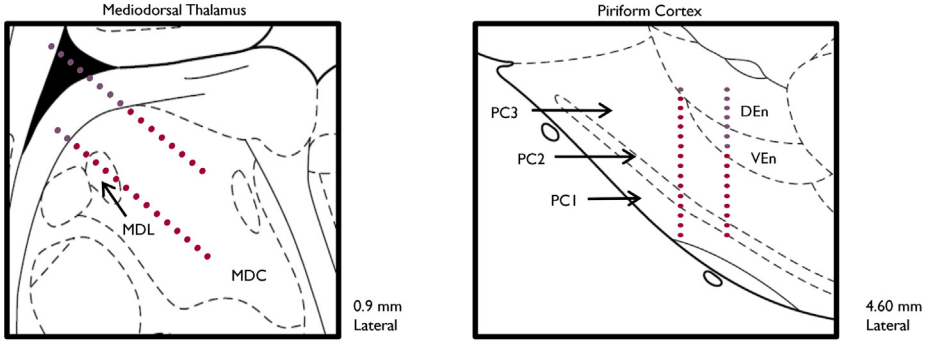

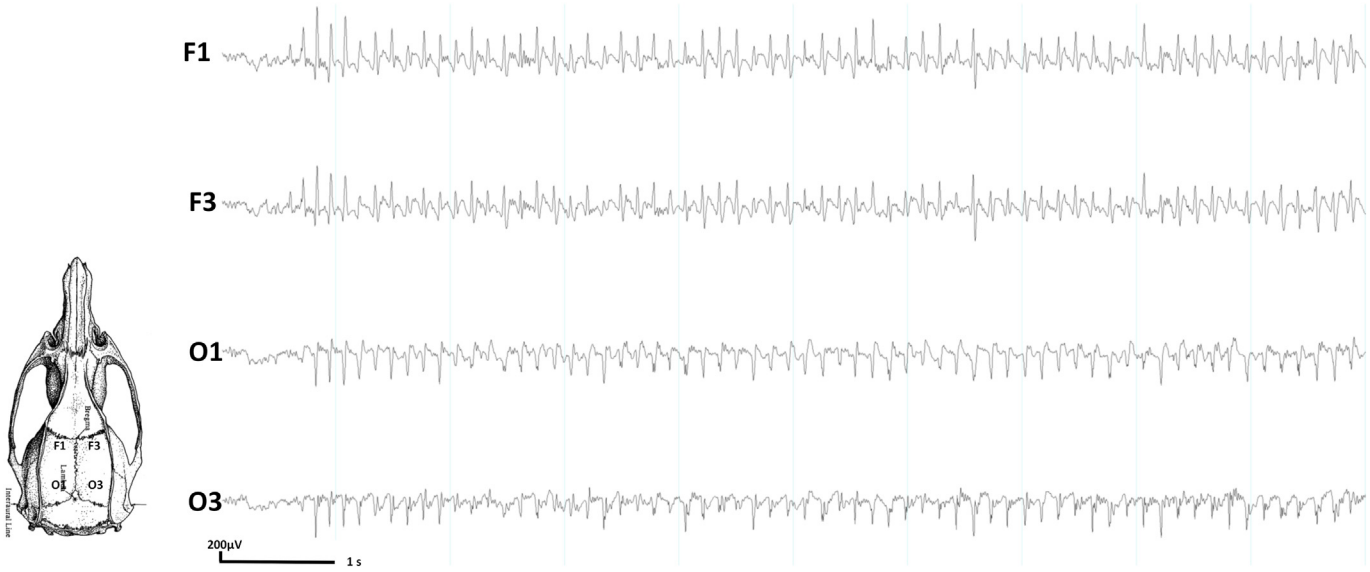

Fig. 2. Cortical EEG recordings of generalized spike–wave discharges recorded from an awake freely moving adult GAERS. Ten seconds window, bandpass filtered 1–100 Hz. F1 — left primary somatosensory cortex; F3 — right primary somatosensory cortex; O1 — left primary visual cortex; O3 — right primary visual cortex.

line in Fig. 4B.

$$A = \int_{\tau_{min}}^{\tau_{max}} Z_{AB}(\tau) - 4\, d\tau \tag{5}$$

A profile of neural synchrony over time can now be constructed by assembling the overall neural synchrony estimates A for each sliding window (10 ms steps) of the time series as shown in Fig. 4C.

3.3. Spike-LFP phase locking

Spike-LFP phase locking is used to determine the relationship a single or MUA has with specific field potential frequency bands. This can be applied as a measure of short-range connectivity by observing changes in phase angle difference of multiunit cluster spikes and field potentials recorded from the same brain region using a microelectrode array. Alternatively, it can be used as a measure of long-range connectivity by observing changes in phase angle difference between MUA in one brain region and the LFPs in another.

3.3.1. Preprocessing

In order to determine the relationship between multiunit cluster spikes and field potentials, both data sets need to be transformed into a phase-based time series. Local field potentials initially undergo zero-phase third-order Butterworth bandpass filtering of the frequency band of interest (e.g., 4–8 Hz for theta). The filtered LFPs then undergo a Hilbert transform followed by a conversion to radians to extract their temporal phase information. Multiunit cluster spikes are assumed to be instantaneous events and, therefore, can be assumed to be equal to π at the time they occur while all other time points are equal to 0. These preprocessing steps are shown in Fig. 5B for a single multiunit cluster spike.

3.3.2. Phase locking value

The phase locking value (PLV) is a commonly used statistic measure of neural synchronization with 0 indicating no synchronization and 1 for indicating complete synchronization [49]. It is also known as intersite phase clustering [50] or mean phase coherence [51]. The PLV determines the degree of clustering in the polar space of phase angle differences. It is symmetric in nature and, therefore, there is no directional information provided. When this method is applied to two phase angle signals from two electrode sites over 16 trials, the PLV can calculate the average of phase angle differences between electrodes over time [52].

$$PLV_f = \left| n^{-1} \sum_{t=1}^{n} e^{i(\phi_{xt} - \phi_{yt})} \right| \tag{6}$$

N is the number of trials, f is the frequency range, t is trial number (1–16), x and y are the two electrode sites, and ϕ_x and ϕ_y are the phase angles of the multiunit spike train and the filtered LFP signal at a specific time point. Because of the instantaneous nature of multiunit spikes, we can assume ϕ_x is equal to π for all spikes and 0 otherwise. For a single multiunit spike, 16 estimates of the PLV can be obtained from the corresponding LFP signals. Hence, the spike-LFP phase locking for a single multiunit cluster spike can be written as follows:

$$SPL_f = \left| n^{-1} \sum_{t=1}^{n} e^{i(\pi - \phi_{yt})} \right|. \tag{7}$$

It is important to note that spike-LFP phase locking can only be calculated for phase angle differences, which display statistically significantly nonuniformity. The Ajne's Test for Nonuniformity is applied to determine whether the 16 phase angle differences satisfy

Fig. 1. Electrode implantation sites. A) Mediodorsal Thalamus Electrode Placement from Coronal Slices — representations of placements (left, image adapted from Paxinos & Watson [42]) and 10× photomicrographs of placement sites from a representative subject. B) Piriform Cortex Electrode Placement from Coronal Slice — representations of placements (left, image adapted from Paxinos & Watson [42]) and photomicrograph of placement sites from a representative subject (left, 4 compiled images taken at 4×; right, image taken at 10×). C) Electrode Placement from Sagittal View Reconstruction. Legend: red arrow/line — microelectrode array track, blue arrow — landmarks granule dentate gyrus (A) and rhinal fissure (B), red dots — represent electrode track line, MDL — mediodorsal thalamus (lateral), MDC — mediodorsal thalamus (central), mediodorsal thalamus (medial), PC1 — piriform cortex layer I, PC2 — piriform cortex layer II, PC3 — piriform cortex layer III, DEn — dorsal endopiriform cortex, VEn — ventral endopiriform cortex.
(From Young JC, Paolini AG, Pedersen M, Jackson GD. Genetic Absence Epilepsy: Effective connectivity of the thalamus, piriform cortex and motor cortex. Currently under review in Epilepsy & Behavior).

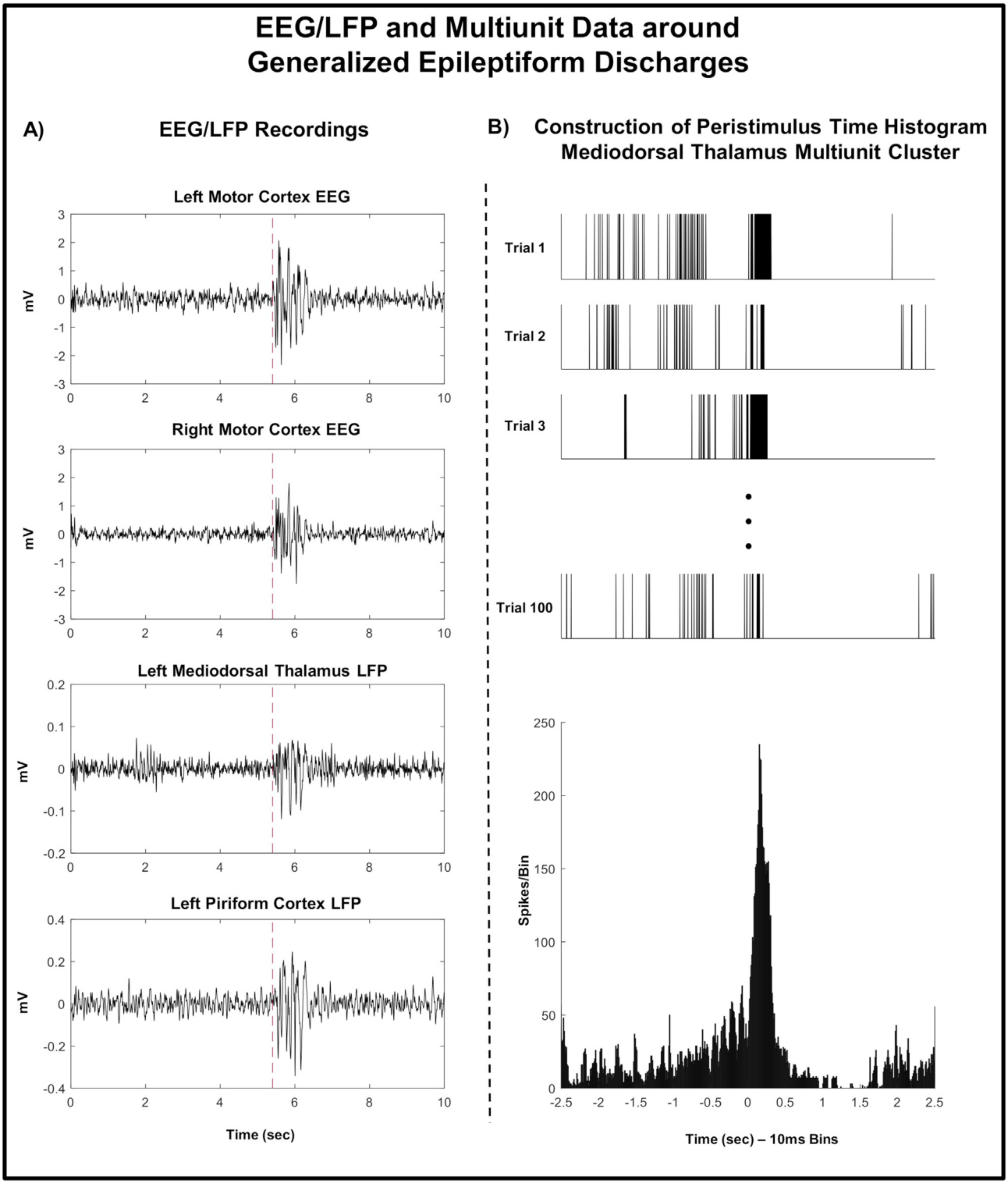

Fig. 3. Raw EEG/LFP and multiunit spike data. A) Generalized epileptiform discharge example across all recording sites. Red dotted line indicates the onset of the generalized epileptiform discharge. B) Construction of peristimulus time histogram from mediodorsal thalamus multiunit cluster. Trial 1 spike train coincides with the left mediodorsal thalamus LFP recording in A). Over 100 trials of the same multiunit cluster, the peristimulus time histogram can be constructed.

this condition (see Section 3.4.2). If the phase angle differences are uniform, then, the multiunit spike is disregarded from the analysis.

3.3.3. Construction of time series

In a similar fashion to the spike rate and neural synchrony analysis, 100 trials of epileptic and control states are utilized for each multiunit cluster in the spike-LFP phase locking analysis. To capture transient changes in the phase locking strength of multiunits to field potentials, a sliding window approach was applied. This time series was constructed with windows of 500 ms duration, 100 ms intervals over 2.5 s (2.5 s prior to discharge onset until point of onset). The longer duration in window size is necessary to capture a sufficient number of multiunit cluster spikes.

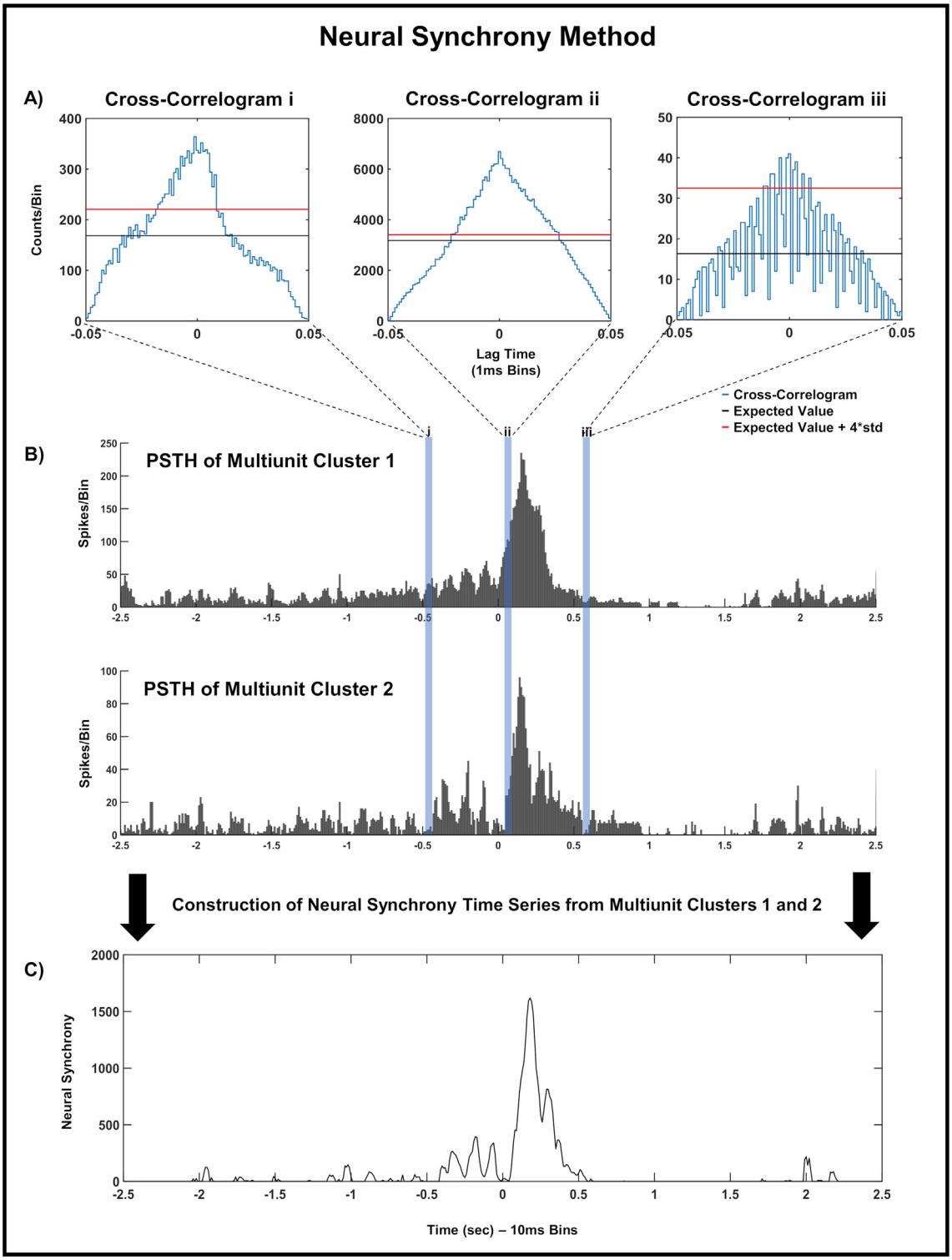

Fig. 4. Neural synchrony method. A) Cross-correlograms for 3 sample 50 ms windows (i, ii, iii). i) Multiunit cluster pair is significantly synchronous with 28.3 ms window of synchronous activity; ii) Multiunit cluster pair is highly synchronous with 48.4 ms window of synchronous activity; iii) Multiunit cluster pair is not significantly synchronous. B) Peristimulus time histograms (PSTH) of a two multiunit clusters around a generalized epileptiform discharge with corresponding cross-correlogram windows i, ii, and iii. C) Constructed neural synchrony time series utilizing the area under the curve of the Z-score of significantly synchronous cross-correlograms.

3.4. Statistics

3.4.1. Spike rate and neural synchrony time series

The Wilcoxon Rank Sum Test was applied to each bin of the overall PSTHs of the PC and MDT, comparing between strains. The Wilcoxon Rank Sum Test was used instead of a paired t-test because of the non-normal distribution of spike rate results. The Wilcoxon Rank Sum Test was also conducted on the neural synchrony time series profiles of the epileptic and control multiunit clusters in a similar fashion. This was conducted for synchrony within the MDT, within the PC, and between

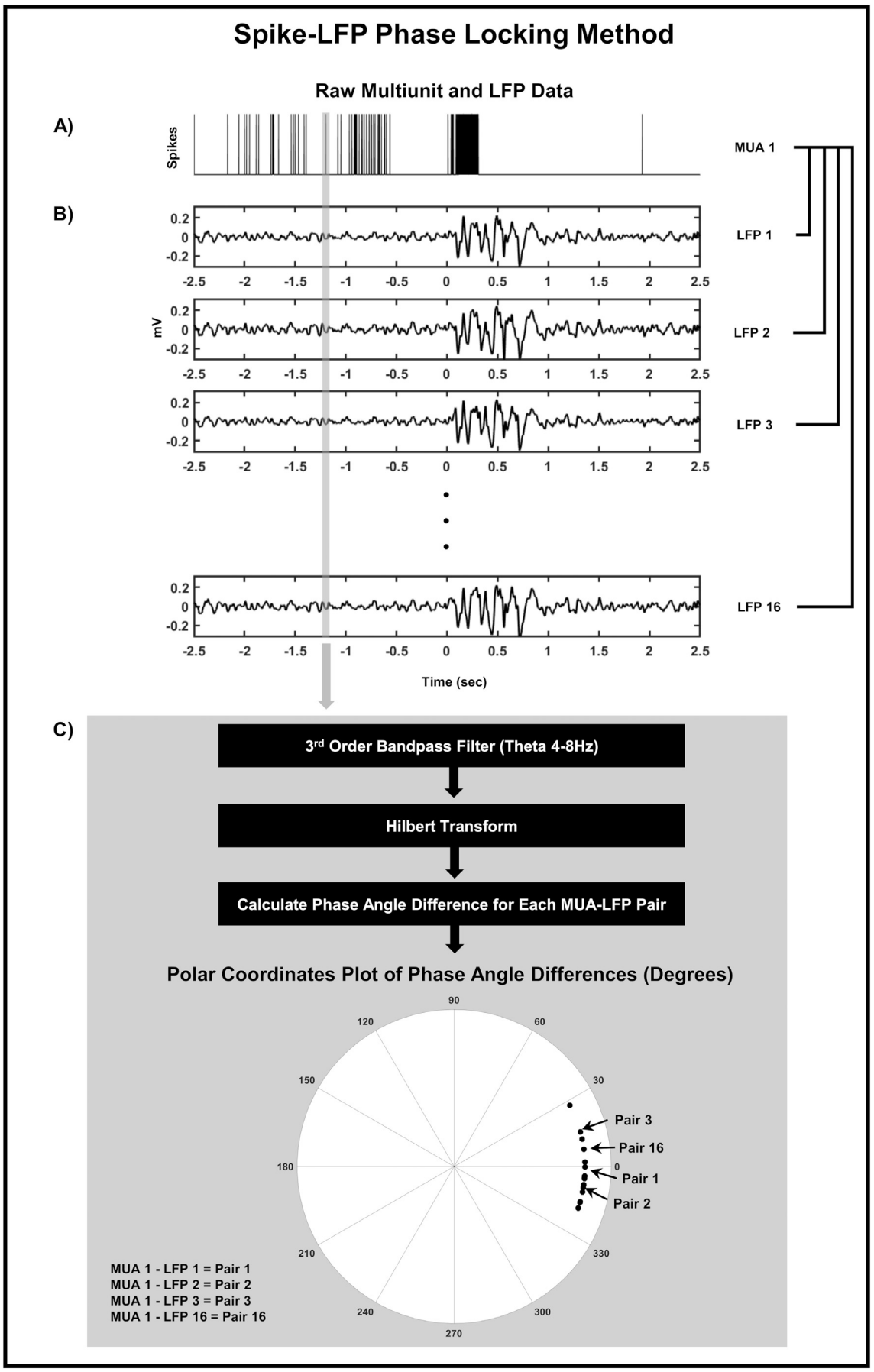
Spike-LFP Phase Locking Method
Raw Multiunit and LFP Data
A)
B)
Spikes
MUA 1
LFP 1
LFP 2
LFP 3
LFP 16
mV
0.2
0
-0.2
-2.5 -2 -1.5 -1 -0.5 0 0.5 1 1.5 2 2.5
Time (sec)
C)
3rd Order Bandpass Filter (Theta 4-8Hz)
Hilbert Transform
Calculate Phase Angle Difference for Each MUA-LFP Pair
Polar Coordinates Plot of Phase Angle Differences (Degrees)
90
120
60
150
30
180
0
210
330
240
300
270
Pair 3
Pair 16
Pair 1
Pair 2
MUA 1 - LFP 1 = Pair 1
MUA 1 - LFP 2 = Pair 2
MUA 1 - LFP 3 = Pair 3
MUA 1 - LFP 16 = Pair 16

the two regions. Z-statistics for all Wilcoxon Rank Sum tests are included in the Supplementary material. The time point of maximum rate or synchronization for each multiunit cluster pair is termed the "peak rate time" and "peak synchronization time", respectively. A Kruskal–Wallis Test was applied to analyze differences in peak rate time for the two brain regions and peak synchronization times for multiunit cluster pairs within the MDT, within the PC, and between the two brain regions followed by a Dunn–Sidak correction (nonparametric post hoc analysis).

3.4.2. Ajne's test for nonuniformity

Prior to the calculation of PLV, it is important to determine that the 16 phase angle difference estimates are significantly nonuniformly distributed. Previous multiunit spike and LFP analyses have utilized the Rayleigh test to test for nonuniformity [18]. However, the Rayleigh test assumes that the distribution of both real and imaginary parts of the phase angle differences are Gaussian distributed. In this study, we have utilized the Ajne's Test, which is nonparametrically equivalent to the Rayleigh Test [53]. For the Rayleigh Test, a minimum of 10 phase angle samples is required [54]. We therefore assume that 16 phase angle samples are sufficient for the Ajne's Test, which is typically applied to sample size less than 50. Multiunit cluster spikes with corresponding phase angle differences that are significantly nonuniform can proceed to have their PLV calculated while nonsignificant multiunit cluster spikes are disregarded.

3.4.3. Spike-field phase locking time series

The spike-LFP phase locking analysis was conducted for PC multiunit phase locking to PC LFPs and MDT multiunit phase locking to MDT field potentials to understand local changes. For observing changes in communication between the two brain regions, MDT multiunit phase locking to PC LFPs was also analyzed. A Wilcoxon Rank Sum Test was conducted separately between the 48 multiunit pairs of the epileptic compared with the controls over the 2.5-second time series to determine if there was a significant difference between the two strains prior to the onset of epileptiform discharges.

For the analysis of the spike-LFP phase locking within the preonset period of −2.5 to 0 s, the Friedman's test of variance was applied because of the results being non-normally distributed. This was done for all 48 multiunit clusters over the 26 segments of the time series (500 ms duration, 100 ms intervals over 2.5 s) followed by a Dunn–Sidak correction (nonparametric post hoc analysis) between the different time series segments. The purpose of this statistical method was to determine if there were significant changes between time points in the spike-LFP phase locking time series prior to the onset of generalized epileptiform discharges.

4. Results

4.1. Peristimulus time histogram

There are distinct patterns of excitation and suppression of MUA prior to and during the onset of generalized epileptiform discharges on the cortical EEG, as displayed in Fig. 6. There are significant increases in the number of spikes/bin at onset for both MDT and PC multiunit clusters ($p < 0.05$, Z values displayed in Fig. 1 in the Supplementary material, Wilcoxon Rank Sum Test). This is followed by a period of inhibition. There is a significant suppression of MUA at several time points prior to the onset of the generalized epileptiform discharge in the PC, however, this is not the case for the MDT ($p < 0.05$, Z-statistic values displayed in Fig. 1 in the Supplementary material, Wilcoxon Rank Sum Test). The median peak spike rate in the MDT occurs at 145.5 ms while the median peak spike rate in the PC occurs at 148 ms for the 48 multiunit clusters. There was no significant difference between the peak spike rate times of the MDT and PC ($p = 0.5047$, $Z = 0.5047$, Wilcoxon Rank Sum Test).

4.2. Patterns of synchronous firing

The transient changes in the strength of neural synchrony are displayed in Fig. 7A. There are significant increases in the strength of neural synchrony ($p < 0.05$, Z-statistic values are displayed in Fig. 2 in the Supplementary material, Wilcoxon Rank Sum Test) during the onset of generalized epileptiform discharge for MDT multiunit cluster pairs, PC multiunit cluster pairs as well as for multiunit cluster pairs between the two brain regions. The median peak synchronization in the MDT occurs at 170 ms, in the PC at 240 ms, and between the two regions at 220 ms. These peaks in synchronization are significantly different from one another ($F(2/905) = 1.192e06$, $p < 0.001$, Kruskal–Wallis Test). Peak synchronization in the MDT is significantly earlier than peak synchronization in the PC ($p < 0.0001$, Dunn–Sidak post hoc test), and peak synchronization between the two regions is also significantly earlier than the PC ($p = 0.0257$, Dunn–Sidak post hoc test). However, the peak synchronization in the MDT is not significantly earlier than the peak synchronization between both regions ($p = 0.0721$). These periods of synchronization are followed by a decrease in the strength of neural synchrony. The fraction of significantly synchronous multiunit cluster pairs over time is displayed in Supplementary material Fig. 3.

4.3. Spike-LFP phase locking

The transient changes in spike-LFP phase locking for each of the different frequency bands and spike-LFP combinations are shown in Fig. 8A for GAERS and NEC strains. This is for the preonset period of −2.5 to 0 s, with circles and error bars indicating the median estimate and interquartile ranges, respectively. All asterisks indicate $p < 0.001$ for pairwise comparisons using Wilcoxon Rank Sum Test over the sliding window time series. Z-statistic values are included in Fig. 4 of Supplementary material.

The changes in spike-LFP phase locking between sliding windows of the preonset time series are displayed in Fig. 8A. There was a significant effect of time on MDT multiunit phase locking to MDT LFPs in the theta band ($\chi^2(25) = 163.82$, $p < 0.0001$) with a significant increase occurring between −2 and −0.5 s. There was no significant effect of time in the beta or gamma band. For PC multiunit phase locking to PC LFPs, there was a significant effect of time for theta ($\chi^2(25) = 91.84$, $p < 0.0001$), beta ($\chi^2(25) = 192.98$, $p < 0.0001$), and gamma ($\chi^2(25) = 198.45$, $p < 0.0001$). In beta and gamma bands, there is a prominent increase in phase locking in the second prior to the generalized epileptiform discharge. There was a significant effect of time on the MDT multiunit phase locking to PC LFPs for the theta ($\chi^2(25) = 55.90$, $p < 0.0001$) and gamma bands ($\chi^2(25) = 74.70$, $p < 0.0001$) with an increase in phase locking occurring prior to the onset of the generalized epileptiform discharge.

5. Discussion

5.1. Suppression–excitation–suppression pattern

We found a dramatic increase in multiunit cluster firing in the MDT during absence seizures. This increase in firing rate after seizure onset

Fig. 5. Spike-LFP methods. A) A multiunit cluster spike train (MUA 1) from the mediodorsal thalamus displays multiunit firing around a generalized epileptiform discharge. B) Field potential signals from the piriform cortex, LFP 1, LFP 2, LFP 3 … LFP 16. The shade gray rectangle overlapping MUA 1 and LFP 1 to LFP 16 is a sample time window of 10 ms around a single spike in MUA 1. C) Signal processing steps. The phase angle difference between the LFP signals and MUA 1 can be determined by bandpass filtering (theta (4–8 Hz) is this example) followed by a Hilbert transform to produce an instantaneous phase time series allowing for the calculation of phase angle differences. The relevant phase angle differences for each MUA-LFP pair can be displayed in their polar coordinates and can be substituted into Eq. (7) to calculate the spike-LFP phase locking value.

was expected as this is typical of higher-order thalamic nuclei [25]. A similar pattern of firing also occurred in the PC. Prior to this excitation, there are several instances of significantly suppressed neuronal activity in both the MDT and PC (Figs. 6A and 5B). Following the excitation, there is a sustained period of suppression. This pattern of neuronal firing suggests dysfunction in excitatory and inhibitory systems within the PC and MDT in this model of absence epilepsy.

Absence epilepsy is thought to be driven by an imbalance inhibition and excitation in thalamocortical microcircuitry [55,56] resulting in instances of hypersynchronized activity which may explain the observations of multiunit cluster firing at epileptiform discharge onset [24]. The MDT has previously exhibited a higher population glutamate positive neurons in GAERS compared with controls [27]. The increased number of glutamate positive neurons may therefore cause corticothalamic hyperexcitability in GAERS. Corticothalamic hyperexcitability is considered to be one of the key forms of neuronal dysfunction in absence epilepsy along with enhanced tonic gamma-Aminobutyric acid ($GABA_A$) inhibition and rhythmical cycling of activity in T-type calcium channels that characterize the oscillatory behavior of absence seizures [57,58].

The MDT and PC may contribute to absence seizure generation because of alterations in their $GABA_A$ inhibition. Gamma-Aminobutyric acid signaling in absence epilepsy is abnormal [59] and involves consistent enhancement of extrasynaptic tonic $GABA_A$ inhibition in the ventrobasal thalamus [60,61]. Interestingly, $GABA_A$ inhibition within the MDT and PC has been previously observed in kindling models of temporal lobe epilepsy [62–64]. This is due to hyperexcitability induced in thalamocortical circuits following kindling of limbic structures and alludes to the possibility of both the MDT and PC displaying abnormal $GABA_A$ inhibition in absence epilepsy. Furthermore, the hyperexcitability of thalamocortical circuits may also have downstream effects via projections of the orbitofrontal cortex to deep pyramidal cells on layer III of the PC [34]. This, in turn, may result in increased glutamatergic communication from the PC to the MDT, further contributing to the manifestation of seizure activity in absence epilepsy via another hyperexcitable circuit. Furthermore, our results demonstrate a noticeably greater suppression of activity in the PC (55.56% of preonset period) compared with the MDT (11.8% of preonset period). This may be the result of tonic inhibition in thalamocortical circuits causing downstream inhibition in the PC. This suppressive effect in the MDT may be less pronounced because of the higher population of glutamatergic positive neurons.

5.2. Synchronization of multiunit activity

Accompanied with increases in excitation at the onset of generalized epileptiform discharges, there is also a significant increase in neural synchrony. This occurred within the PC and MDT as well as between the two regions, demonstrating hypersynchronous activity. Peaks of synchronous activity are shown to occur after the onset of the generalized epileptiform discharges in line with the Meeren et al. hypothesis of a cortical focus driving absence seizures [20,41,65]. The earliest peak of synchronous activity observed in our study was in the MDT. The PC is more delayed in its synchronous firing of multiunit clusters, suggesting

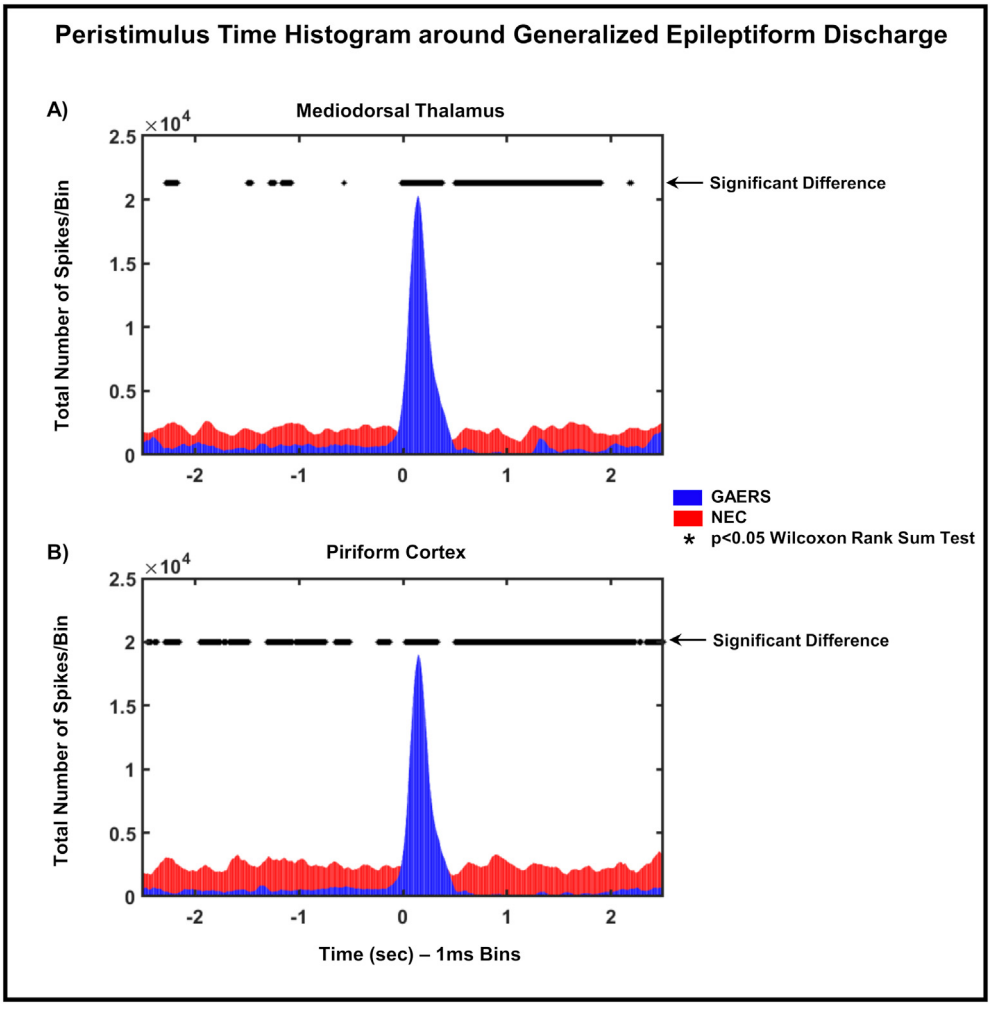

Fig. 6. Peristimulus time histogram (PSTH) of GAERS and NEC multiunit cluster. A) Total PSTH of mediodorsal thalamus. B) Total PSTH of piriform cortex. Asterisks above PSTHs represent instances of significant difference between the PSTHs of GAERS and NEC strains. The corresponding Z-statistics plots are in Supplementary Fig. 1.

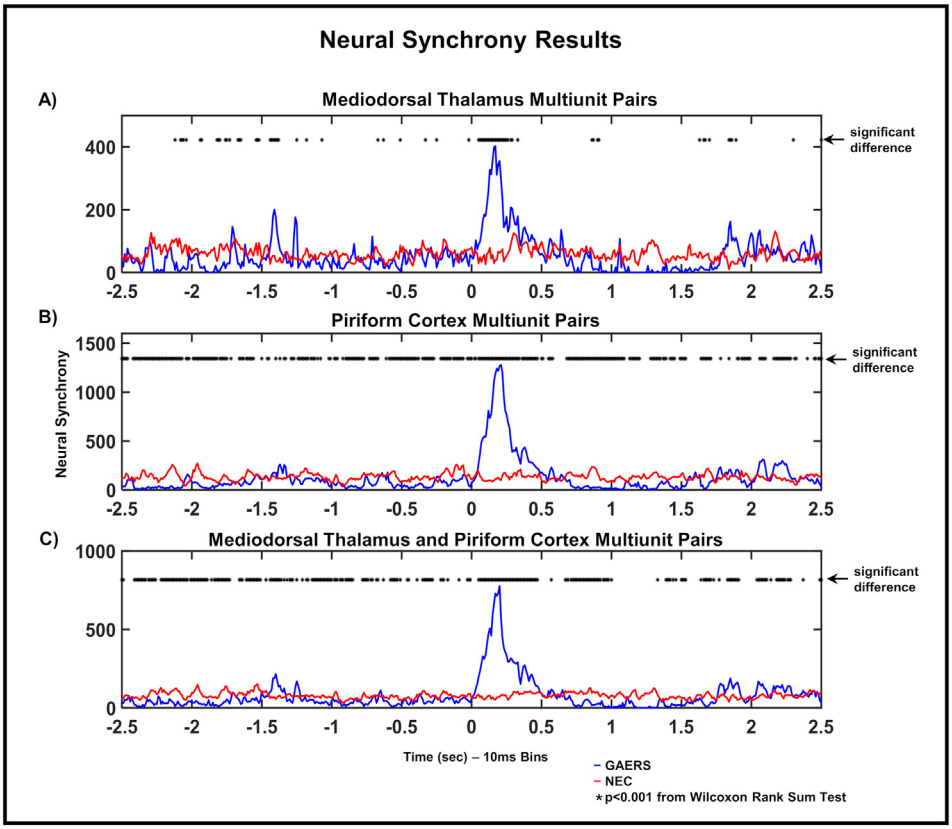

Fig. 7. Neural synchrony results. Neural synchrony time series profile based on area under the curve of the cross-correlogram Z-score and Z = 4. A) Neural synchrony within mediodorsal thalamus. B) Neural synchrony within piriform cortex. C) Neural synchrony between the mediodorsal thalamus and piriform cortex. Significant changes in neural synchrony profile indicated by asterisks ($p < 0.001$, Z-statistics in Fig. 2 of Supplementary material, Wilcoxon Rank Sum Test).

that it is later involved in the spread of the discharges compared with the MDT. Peak synchronous firing between the two brain regions occurs later than the MDT but earlier than the PC. This suggests that the engagement of communication between the PC and MDT is driven by the MDT's downstream relationship with cortical structures such as the orbitofrontal cortex, rather than the PC dictating the flow of information. Therefore, synchronous activity in the PC may be the result of recruitment of the PC to MDT pathway.

Prior to the onset of generalized epileptiform discharges, there is significantly less synchronous activity during large portions of the preonset period for synchrony within PC and between the two regions, and is less so for the MDT. This decrease in PC synchrony may be the result of increased inhibition because of cortical influences as observed in the PSTHs. Communication between the PC and MDT is typically excitatory, therefore, a reduction in synchronous firing between these regions may also reflect an inhibitory process occurring [16].

5.3. Spike-LFP phase locking

Evidence to support the hypothesis of an imbalance in excitation and inhibition in the pathophysiology of absence seizures is displayed in the spike-LFP phase locking within the PC and MDT as well as between the two regions. There is a distinct pattern of oscillatory activity in the theta band for the MDT resulting in a decrease in spike-LFP phase locking at −0.5 s. This decrease corresponds to peaks across all PC spike-LFP phase locking frequency bands as well as a decrease and increase in the phase locking of MDT multiunits to PC field potentials for theta and gamma bands, respectively.

5.3.1. Theta

There are notable fluctuations in the spike-LFP phase locking in the theta band of the MDT with a distinct decrease at −0.5 s. This effect may be due to the functionality of T-type calcium channels in the MDT changes prior to discharge onset. T-type calcium channels are known to play a key role in the generation and maintenance of absence seizures [66]. An increase in bursting activity in the MDT during theta frequency interactions has shown to depend on T-type calcium channels [67]. This was found to occur following hypoxic-like damage to the prefrontal cortex as a model of frontal lobe epilepsy. Kim et al. proposed that inhibitory mechanisms resulting in the deactivation of T-type calcium channels in the MDT may be achieved via feedback mechanisms between the reticular thalamic nuclei and the prefrontal cortex [68,69]. The reticular thalamic nuclei can produce absence seizures via the slow kinetics of inhibitory $GABA_B$ receptors [70,71] and have also been utilized a deep brain stimulation target in the treatment of absence seizures [72]. Therefore, abnormal interactions between these two thalamic nuclei may modulate T-type calcium channels in the MDT resulting in fluctuations in the spike-LFP phase locking in the theta band and suppression of neuronal firing prior to the onset of generalized epileptiform discharges. Alternatively, the MDT could also be influenced by the orbitofrontal cortex or dorsolateral prefrontal cortex inputs because of their involvement in the absence epilepsy network [73,74]. The dorsolateral prefrontal cortex has previously displayed peaks in blood oxygen-level dependent (BOLD) response from EEG/fMRI approximately 2 s prior to absence seizures onset, suggesting an early involvement in their generation [75].

The sharp decrease in the phase locking MDT multiunits to PC field potentials illustrates dysfunction within theta oscillatory communication from the PC to the MDT. Prior to this decrease, the spike-LFP phase locking is relatively stable, suggesting that this decrease is the

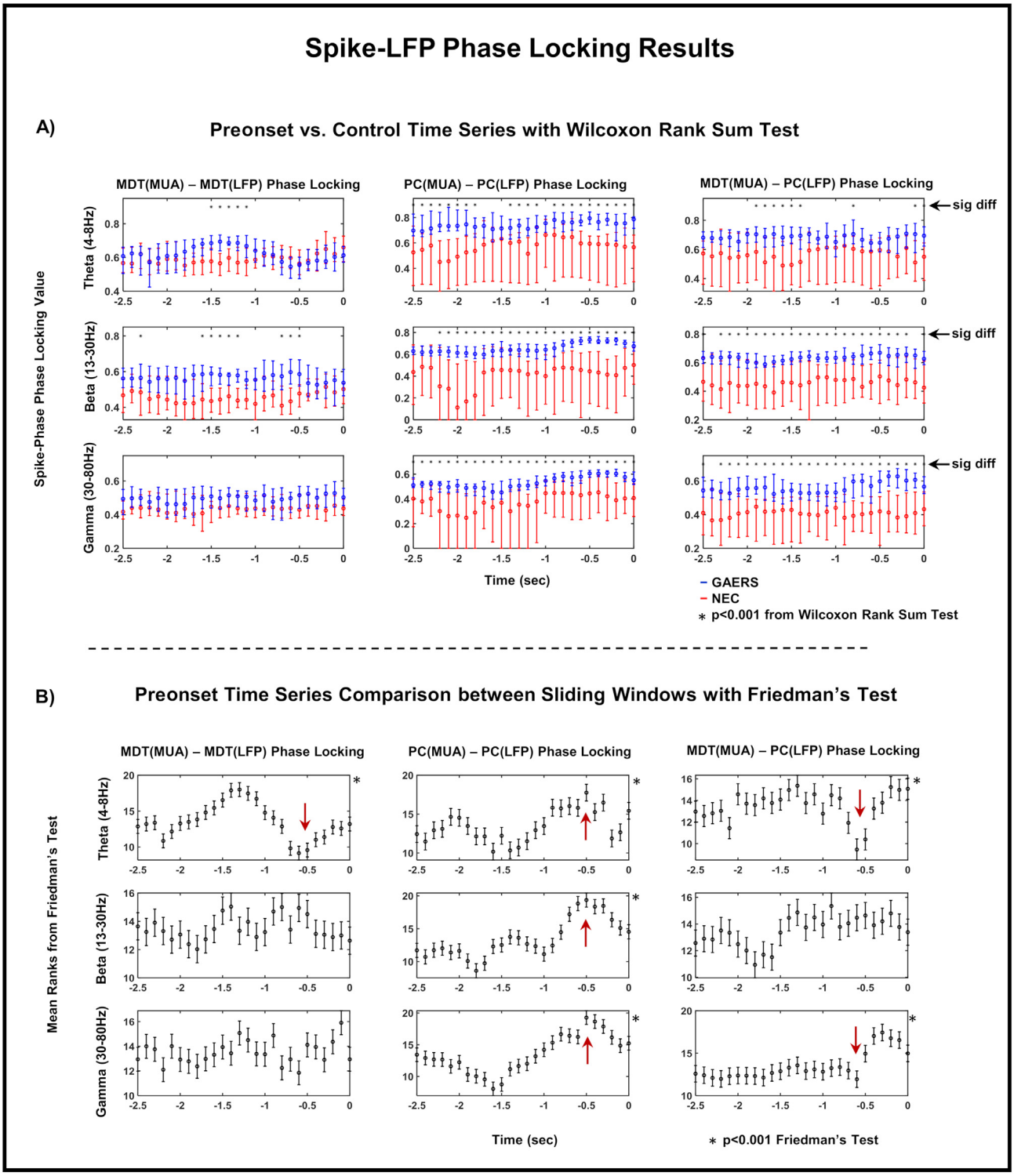

Fig. 8. Spike-LFP phase locking results. A) Comparison of preonset time series (2.5 s prior to onset of epileptiform discharge) and control time series of spike-LFP phase locking using Wilcoxon Rank Sum Test (*$p < 0.001$, sig diff = significant difference). Error bars are interquartile ranges due to non-normal distribution of results. Left column is the spike-LFP phase locking of mediodorsal thalamus multiunits to mediodorsal thalamus field potentials (MDT(MUA)-MDT(LFP)), middle column is the spike-LFP phase locking of piriform cortex multiunits to piriform cortex field potentials (PC(MUA)-PC(LFP)), and right column is the spike-LFP phase locking of mediodorsal thalamus multiunits to piriform cortex field potentials (MDT(MUA)-PC(LFP)). Top row is spike-LFP phase locking in theta band (4–8 Hz), middle row is spike-LFP phase locking in beta band (13–30 Hz), and bottom row is spike-LFP phase locking in gamma band (30–80 Hz). Corresponding Z-statistics in Supplementary Fig. 4. B) Comparison between time points of preonset time series using Friedman's test. Asterisks indicate $p < 0.001$ for Friedman's test, and error bars are pairwise intervals calculated from Dunn–Sidak procedure that indicates $p < 0.05$ for pairwise comparisons. Red arrows indicate important temporal changes at −0.5 s across multiple MUA-LFP plots prior to the onset of the generalized epileptiform discharge.

result of local changes in the MDT, such as dysfunction of T-type calcium channels, resulting in a destabilization of the communication in this neural pathway.

5.3.2. Beta

Beta band spike-LFP phase locking in the PC is shown to peak at approximately −0.5 s coinciding with the respective increases and

decreases in spike-LFP phase locking in PC and MDT theta bands. The degree of spike-LFP phase locking is significantly greater compared with controls after −2.3 s. Beta oscillations are considered to be generated as a result of a feedback system between the olfactory bulb and PC [76,77], however, there is also evidence to suggest that this activity is critical in long range communication between the orbitofrontal cortex, MDT, and PC [78,79]. Therefore, changes in beta spike-LFP phase locking in the PC may be cortically driven by the wider absence epilepsy network rather than changes in the olfactory bulb–PC functionality. There is no noticeable transient change in the spike-LFP phase locking of MDT multiunits to PC field potentials, however, the degree of spike-LFP phase locking in beta is significantly higher compared with controls. Mediodorsal thalamus multiunits and PC field potentials have previously shown to increase in phase locking in response to odor stimuli [18]. While this previous finding is likely due to modulation of the olfactory bulb and PC feedback circuit, our results allude to recruitment of the PC–MDT pathway as part of the absence epilepsy network.

5.3.3. Gamma

There is a similar increase in gamma band spike-LFP phase locking in the PC compared with the beta band. This builds on previous work by our group, which demonstrated on LFP recordings in the somatosensory cortex short-lasting HFOs prior to the spike in each cycle of the spike–wave discharges in GAERS [41]. These local increases in gamma band spike-LFP phase locking may affect the local feedback inhibitory circuits generated by GABAergic basket cells receiving associational axon inputs from pyramidal cells in the PC [19]. An imbalance in excitation and inhibition within the PC may result in dysfunctional gamma oscillatory activity. Because of the pyramidal cells in layer III of the PC projecting directly to the orbitofrontal cortex and downstream to the dorsolateral prefrontal cortex, these local changes in the PC may modulate cortical regions associated with the generation of absence seizures.

Following the increase of spike-LFP phase locking in the PC gamma band at approximately −0.5 s, there is a subsequent rise in spike-LFP phase locking between MDT multiunits and PC field potentials. This also occurs at the same time as the decrease in MDT multiunits phase locking to PC field potentials in the theta band. The spike-LFP phase locking in the gamma band is also significantly higher in the GAERS compared with the NEC following −2.4 s. It can be hypothesized that this rapid increase reflects an excitatory process commencing, due to the excitatory nature of axonal terminals between the two regions [16], potentially contributing to the onset of the absence seizures. This process may be driven by glutamatergic excitation within the PC as well as possible dysfunction of T-type calcium channels in the MDT resulting in a possible positive feedback system aided by cortical regions.

5.4. Limitations

It has been reported that LFPs spread over approximately 250 μm [80], which can be further extended in the presence of stimuli or an event such as a generalized seizure [81], therefore, it is important to acknowledge that the spike-LFP phase locking findings for within the MDT may be influenced by other thalamic nuclei that contribute absence epilepsy such as ventrobasal thalamus or the reticular thalamic nuclei [42]. This is unlikely the case for the within PC spike-LFP phase locking results as it is anatomically distal (>5 mm) from cortical regions critically involved in absence epilepsy [42]. Furthermore, this issue is not applicable to the spike-LFP phase locking of MDT multiunits with PC field potentials because of their anatomical distance (>5 mm) [42].

6. Conclusions

The subcortical influences on seizure onset in absence epilepsy remain a mystery and are typically disregarded because of the cortical driven hypothesis of absence epilepsy. However, our findings have demonstrated that there are distinct early changes in spike-LFP phase locking within neural oscillatory bands associated with communication between the PC and MDT prior to the onset of epileptic activity. This neural pathway may therefore contribute to absence seizure initiation, however, it is unclear whether it plays an active role like the somatosensory cortex–ventrobasal thalamus pathway. Future studies should endeavor to investigate the interactions between PC and MDT with other structures such as the somatosensory cortex, ventrobasal thalamus, orbitofrontal cortex, or dorsolateral prefrontal cortex to determine whether they are involved in large-scale brain networks associated with absence epilepsy.

Author contributions

Authors had full access to all data and take responsibility of the presented data. Prof. Antonio G. Paolini and James C. Young designed and performed the experiments together. James Young analyzed all of the data acquired. All authors interpreted the data and were involved in drafting and revising of the article with respect to intellectual content. The study was supervised by Prof. Antonio Paolini and Prof. Graeme D Jackson.

Declaration of Competing Interest

The authors declare that the research was conducted in the absence of any commercial or financial relationship that could be construed as a potential conflict of interest.

Acknowledgments

We thank Angela Lim for assistance in electrophysiology recording monitoring and aiding in transcardial perfusion. The Florey Institute of Neuroscience and Mental Health acknowledges the strong support from the Victorian Government in particular the funding from the Operational Infrastructure Support Grant. This study was supported by the National Health and Medical Research Council of Australia (NHMRC Project Grant #1091593 and NHMRC Program Grant #1091593). James C Young acknowledges that they have been supported through an Australian Government Research Training Program Scholarship. Pablo Casillas-Espinosa works is funded by the Peter Doherty Early Career Fellowship (NHMRC# APP1166170).

References

[1] Tondelli M, Vaudano AE, Ruggieri A, Meletti S. Cortical and subcortical brain alterations in juvenile absence epilepsy. NeuroImage Clin 2016;12:306–11.
[2] Löscher W, Ebert U. The role of the piriform cortex in kindling. Prog Neurobiol 1996; 50:427–81.
[3] Vaughan D, Warren A, Carney P, Abbott D, Archer J, Jackson G. Timing and laterality of piriform cortex activation in focal and generalized epilepsies. Honolulu, Hawaii: 21st Organization for Human Brain Mapping Conference; 2015.
[4] Vaughan DN, Jackson GD. The piriform cortex and human focal epilepsy. Front Neurol 2014;5:1–18.
[5] Vismer MS, Forcelli PA, Skopin MD, Gale K, Koubeissi MZ. The piriform, perirhinal, and entorhinal cortex in seizure generation. Frontiers In Neural Circuits 2015;9:27.
[6] Galovic M, Baudracco I, Wright-Goff E, Pillajo G, Nachev P, Wandschneider B, Woermann F, Thompson P, Baxendale S, McEvoy A, Nowell M, Mancini M, Vos S, P. Winston G, Sparks R, Prados F, Miserocchi A, de Tisi J, André Van Graan L, J. Koepp M. Association of piriform cortex resection with surgical outcomes in patients with temporal lobe epilepsy; 2019.
[7] Arcaro J, Ma J, Chu L, Kuo M, Mirsattari SM, Stan Leung L. The hippocampus participates in a pharmacological rat model of absence seizures. Epilepsy Res 2016;120: 79–90.
[8] Akhmadeev AV, Nagaeva DV, Kalimullina LB. The paleoamygdala: comparative analysis of its structural-functional organization in WAG/Rij and Wistar rats. Neurosci Behav Physiol 2013;682.
[9] Carçak N, Ferrandon A, Koning E, Aker RG, Ozdemir O, Onat FY, et al. Effect of stage 2 kindling on local cerebral blood flow rates in rats with genetic absence epilepsy. Epilepsia 2009;50:33–43.
[10] Onat FY, van Luijtelaar G. Nehlig A. Snead OC: III. The involvement of limbic structures in typical and atypical absence epilepsy. In; 2013 [p. 111-123].
[11] Young JC, Vaughan DN, Paolini AG, Jackson GD. Electrical stimulation of the piriform cortex for the treatment of epilepsy: a review of the supporting evidence. Behavior; Epilepsy Behav 2018;88:152–61.

[12] Cornwall J, Phillipson OT. Afferent projections to the dorsal thalamus of the rat as shown by retrograde lectin transport—I. The mediodorsal nucleus. Neuroscience 1988;24:1035–49.
[13] Powell TPS, Cowan WM, Raisman G. Olfactory relationships of the diencephalon. Nature 1963;199:710.
[14] Price JL. Beyond the primary olfactory cortex: olfactory-related areas in the neocortex, thalamus and hypothalamus. Chem Senses 1985;10:239.
[15] Bay HH, Cavdar S. Regional connections of the mediodorsal thalamic nucleus in the rat. Imperial College Press; 2013; 201.
[16] Kuroda M, López-Mascaraque L, Price JL. Neuronal and synaptic composition of the mediodorsal thalamic nucleus in the rat: a light and electron microscopic Golgi study. J Comp Neurol 1992;326:61–81.
[17] Fukunaga I, Herb JT, Kollo M, Boyden ES, Schaefer AT. Independent control of gamma and theta activity by distinct interneuron networks in the olfactory bulb. Nat Neurosci 2014;17:1208–16.
[18] Courtiol E, Wilson DA. Thalamic olfaction: characterizing odor processing in the mediodorsal thalamus of the rat. J Neurophysiol 2014;111:1274–85.
[19] Mori K, Manabe H, Narikiyo K, Onisawa N. Olfactory consciousness and gamma oscillation couplings across the olfactory bulb, olfactory cortex, and orbitofrontal cortex. Front Psychol 2013;4.
[20] Meeren HKM, Pijn JPM, Van Luijtelaar ELJM, Coenen AML, Lopes da Silva FH. Cortical focus drives widespread corticothalamic networks during spontaneous absence seizures in rats. J Neurosci Off J Soc Neurosci 2002;22:1480–95.
[21] Westmijse I, Ossenblok P, Gunning B, Luijtelaar GV. Onset and propagation of spike and slow wave discharges in human absence epilepsy: a MEG study. Epilepsia 2009; 50:2538–48.
[22] Inoue M, Duysens J, Vossen JMH, Coenen AML. Thalamic multiple-unit activity underlying spike–wave discharges in anesthetized rats. Brain Res 1993;612:35–40.
[23] Blumenfeld H. Cellular and network mechanisms of spike–wave seizures. Epilepsia 2005;46(Suppl. 9):21–33.
[24] Pinault D, O'Brien T. Cellular and network mechanisms of genetically-determined absence seizures; 2005.
[25] Seidenbecher T, Pape H-C. Contribution of intralaminar thalamic nuclei to spike-and-wave-discharges during spontaneous seizures in a genetic rat model of absence epilepsy. Eur J Neurosci 2001;13:1537–46.
[26] Zhang CH, Sha Z, Mundahl J, Liu S, Lu Y, Henry TR, et al. Thalamocortical relationship in epileptic patients with generalized spike and wave discharges — a multimodal neuroimaging study. NeuroImage Clinical 2015;9:117–27.
[27] Çavdar S, Özgür M, Kirazlı Ö, Karahüseyinoğlu S, Onat F. Comparing glutamatergic neuron population in the mediodorsal thalamic nucleus of genetic absence epilepsy rats from Strasbourg (GAERS) and normal control Wistar rats. J Chem Neuroanat 2016;77:93–9.
[28] Marescaux C, Vergnes M, Depaulis A. Genetic absence epilepsy in rats from Strasbourg—a review. J Neural Transm Suppl 1992;35:37–69.
[29] Depaulis A, David O, Charpier S. The genetic absence epilepsy rat from Strasbourg as a model to decipher the neuronal and network mechanisms of generalized idiopathic epilepsies. J Neurosci Methods 2016;260:159–74.
[30] Kelemen A, Barsi P, Gyorsok Z, Sarac J, Szűcs A, Halász P. Thalamic lesion and epilepsy with generalized seizures, ESES and spike–wave paroxysms—report of three cases. Seizure 2006;15:454–8.
[31] Barbas H, García-Cabezas MÁ, Zikopoulos B. Frontal-thalamic circuits associated with language. Brain Lang 2013;126:49–61.
[32] Zelano C, Mohanty A, Gottfried JA. Olfactory predictive codes and stimulus templates in piriform cortex. Neuron 2011;178.
[33] Parnaudeau S, Bolkan SS, Kellendonk C. The mediodorsal thalamus: an essential partner of the prefrontal cortex for cognition. Biol Psychiatry 2018;83:648–56.
[34] Illig KR. Projections from orbitofrontal cortex to anterior piriform cortex in the rat suggest a role in olfactory information processing. J Comp Neurol 2005;488:224–31.
[35] Bai X, Guo J, Killory B, Vestal M, Berman R, Negishi M, et al. Resting functional connectivity between the hemispheres in childhood absence epilepsy. Neurology 2011; 76:1960–7.
[36] Caplan R, Levitt J, Siddarth P, Wu KN, Gurbani S, Sankar R, et al. Frontal and temporal volumes in childhood absence epilepsy. Epilepsia 2009;50:2466–72.
[37] Holmes MD, Brown M, Tucker DM. Are "generalized" seizures truly generalized? Evidence of localized mesial frontal and frontopolar discharges in absence. Epilepsia 2004;45:1568–79.
[38] Rolls ET. Convergence of sensory systems in the orbitofrontal cortex in primates and brain design for emotion. Anat Rec A Discov Mol Cell Evol Biol 2004;281:1212–25.
[39] David O, Guillemain I, Saillet S, Reyt S, Deransart C, Segebarth C, et al. Identifying neural drivers with functional MRI: an electrophysiological validation. PLoS Biol 2008;6:e315.
[40] Nersesyan H, Hyder F, Rothman DL, Blumenfeld H. Dynamic fMRI and EEG recordings during spike–wave seizures and generalized tonic–clonic seizures in WAG/Rij rats. J Cereb Blood Flow Metab 2004;24:589–99.
[41] Zheng TW, O'Brien TJ, Morris MJ, Reid CA, Jovanovska V, O'Brien P, et al. Rhythmic neuronal activity in S2 somatosensory and insular cortices contribute to the initiation of absence-related spike-and-wave discharges. Epilepsia 2012; 53:1948–58.
[42] Paxinos G, Watson C. The rat brain in stereotaxic coordinates/George Paxinos, Charles Watson. San Diego: Academic Press; 1998 c1998.
[43] Mohit NS. Inferior colliculus responses to multichannel microstimulation of the ventral cochlear nucleus: implications for auditory brain stem implants. J Neurophysiol 2008;99:1–13.
[44] Staba RJ, Wilson CL, Bragin A, Fried I, Engel Jr J. Quantitative analysis of high-frequency oscillations (80–500 Hz) recorded in human epileptic hippocampus and entorhinal cortex. J Neurophysiol 2002;88:1743–52.
[45] Gardner AB, Worrell GA, Marsh E, Dlugos D, Litt B. Human and automated detection of high-frequency oscillations in clinical intracranial EEG recordings. Clin Neurophysiol 2007;118:1134–43.
[46] Tchumatchenko T, Geisel T, Volgushev M, Wolf F. Spike correlations — what can they tell about synchrony? Front Neurosci 2011;5:68.
[47] Futatsugi Y, Riviello Jr JJ. Mechanisms of generalized absence epilepsy. Brain Dev 1998;20:75–9.
[48] Eggermont JJ. Neural interaction in cat primary auditory cortex. Dependence on recording depth, electrode separation, and age. J Neurophysiol 1992;68:1216–28.
[49] Lachaux J-P, Rodriguez E, Martinerie J, Varela FJ. Measuring phase synchrony in brain signals. Hum Brain Mapp 1999;8:194–208.
[50] Cohen MX. Analyzing neural time series data: theory and practice. Cambridge, Massachusetts: The MIT Press; 2014.
[51] Mormann F, Lehnertz K, David P, E. Elger C. Mean phase coherence as a measure for phase synchronization and its application to the EEG of epilepsy patients. In. Netherlands: ELSEVIER; 2000. p. 358.
[52] Lachaux JP, Rodriguez E, Le van Quyen M, Lutz A, Martinerie J, Varela FJ. Studying single-trials of phase synchronous activity in the brain. Great Britain: World Scientific Publishing Co; 2000; 2429.
[53] Ajne B. A simple test for uniformity of a circular distribution. Biometrika 1968;55: 343.
[54] Zar JH. Biostatistical analysis. Prentice Hall; 1999.
[55] Avanzini G, de Curtis M, Franceschetti S, Sancini G, Spreafico R. Cortical versus thalamic mechanisms underlying spike and wave discharges in GAERS. Epilepsy Res 1996;26:37–44.
[56] Dufour F, Nalecz KA, Nalecz MJ, Nehlig A. Metabolic approach of absence seizures in a genetic model of absence epilepsy, the GAERS: study of the leucine–glutamate cycle. J Neurosci Res 2001;66:923–30.
[57] Tringham E, Powell KL, Cain SM, Kuplast K, Mezeyova J, Weerapura M, Eduljee C, Jiang X, Smith P, Morrison J-L, Jones NC, Braine E, Rind G, Fee-Maki M, Parker D, Pajouhesh H, Parmar M, O'Brien TJ, Snutch TP. T-type calcium channel blockers that attenuate thalamic burst firing and suppress absence seizures. In; 2012.
[58] Leresche N, Lambert RC. GABA receptors and T-type Ca2 + channels crosstalk in thalamic networks. In; 2018. p. 37–45.
[59] Pedersen MK, Omidvarnia Magdalena, Perucca Amir, Gooley Piero, Petrou Samuel, Scheffer Steve, et al. Functional brain connectivity is increased in people with a pro-epileptic GABRG2 mutation. Amer Epil Soc Annual Meeting 2018. New Orleans, LA, US; 2018.
[60] Wong M. Too much inhibition leads to excitation in absence epilepsy. Epilepsy Currents 2010;10:131–2.
[61] Cope DW, Di Giovanni G, Fyson SJ, Orbán G, Errington AC, Lőrincz ML, et al. Enhanced tonic GABAA inhibition in typical absence epilepsy. Nat Med 2009;15:1392.
[62] Gavrilovici C, D'Alfonso S, Dann M, Poulter MO. Kindling-induced alterations in GABAA receptor-mediated inhibition and neurosteroid activity in the rat piriform cortex. Eur J Neurosci 2006;24:1373–84.
[63] Rajasekaran K, Sun C, Bertram EH. Altered pharmacology and GABA-A receptor subunit expression in dorsal midline thalamic neurons in limbic epilepsy. Neurobiol Dis 2009;33:119–32.
[64] Richards DA, Lemos T, Whitton PS, Bowery NG. Extracellular GABA in the ventrolateral thalamus of rats exhibiting spontaneous absence epilepsy: a microdialysis study. J Neurochem 1995;65:1674–80.
[65] McCafferty C, David F, Venzi M, Lőrincz ML, Delicata F, Atherton Z, et al. Cortical drive and thalamic feed-forward inhibition control thalamic output synchrony during absence seizures. Nat Neurosci 2018;21:744–56.
[66] Chen Y, Parker WD, Wang K. The role of T-type calcium channel genes in absence seizures. Front Neurol 2014;5:45.
[67] Kim J, Woo J, Park Y-G, Chae S, Jo S, Choi JW, Jun HY, Yeom YI, Park SH, Kim KH, Shin H-S, Kim D. Thalamic T-type Ca2 + channels mediate frontal lobe dysfunctions caused by a hypoxia-like damage in the prefrontal cortex. In; 2011. p. 4063–4073.
[68] Groenewegen HJ. Organization of the afferent connections of the mediodorsal thalamic nucleus in the rat, related to the mediodorsal–prefrontal topography. Neuroscience 1988;24:379–431.
[69] Zikopoulos B, Barbas H. Prefrontal projections to the thalamic reticular nucleus form a unique circuit for attentional mechanisms. J Neurosci 2006;26:7348.
[70] Destexhe A. Spike-and-wave oscillations based on the properties of $GABA_B$ receptors. J Neurosci 1998;18:9099.
[71] Chen M, Guo D, Wang T, Jing W, Xia Y, Xu P, et al. Bidirectional control of absence seizures by the basal ganglia: a computational evidence. PLoS Comput Biol 2014; 10:1–17.
[72] Wang Z, Wang Q. Eliminating absence seizures through the deep brain stimulation to thalamus reticular nucleus. Front Comput Neurosci 2017;11:22.
[73] Carney PW, Masterton RA, Flanagan D, Berkovic SF, Jackson GD. The frontal lobe in absence epilepsy: EEG-fMRI findings. Neurology 2012;78:1157–65.
[74] Klein JC, Rushworth MFS, Behrens TEJ, Mackay CE, de Crespigny AJ, D'Arceuil H, et al. Topography of connections between human prefrontal cortex and mediodorsal thalamus studied with diffusion tractography. Neuroimage 2010;51:555–64.
[75] Szaflarski JP, DiFrancesco M, Hirschauer T, Banks C, Privitera MD, Gotman J, et al. Cortical and subcortical contributions to absence seizure onset examined with EEG/fMRI. Behavior;Epilepsy Behav 2010;18:404–13.
[76] Neville KR, Haberly LB. Beta and gamma oscillations in the olfactory system of the urethane-anesthetized rat. In; 2003. p. 3921–3930.
[77] David F, Courtiol E, Buonviso N, Fourcaud-Trocmé N. Competing mechanisms of gamma and beta oscillations in the olfactory bulb based on multimodal inhibition of mitral cells over a respiratory cycle. eNeuro 2015;2 (ENEURO.0018-15.2015).

[78] Plailly J, Howard JD, Gitelman DR, Gottfried JA. Attention to odor modulates thalamocortical connectivity in the human brain. J Neurosci Off J Soc Neurosci 2008;28:5257–67.
[79] Tallon-Baudry C, Bertrand O, Fischer C. Oscillatory synchrony between human extrastriate areas during visual short-term memory maintenance. J Neurosci 2001;21: RC177.
[80] Katzner S, Nauhaus I, Benucci A, Bonin V, Ringach DL, Carandini M. Local origin of field potentials in visual cortex. In. United States. Amsterdam: Elsevier Science B.V.; 2009; 35.
[81] Kajikawa Y, Schroeder CE. How local is the local field potential? Neuron 2011;72: 847–58.